STRUCTURAL BIOLOGY COMMUNICATIONS

ISSN 2053-230X

Crystal structure of bile salt hydrolase from *Lactobacillus salivarius*

Fuzhou Xu,[a] Fangfang Guo,[a] Xiao-Jian Hu[b]* and Jun Lin[c]*

[a]Beijing Key Laboratory for Prevention and Control of Infectious Diseases in Livestock and Poultry, Institute of Animal Husbandry and Veterinary Medicine, Beijing Academy of Agriculture and Forestry Sciences, Beijing 100097, People's Republic of China, [b]Department of Physiology and Biophysics, School of Life Sciences, Fudan University, Shanghai 200438, People's Republic of China, and [c]Department of Animal Science, The University of Tennessee, Knoxville, TN 37996, USA. *Correspondence e-mail: xjhu@fudan.edu.cn, jlin6@utk.edu

Received 25 January 2016
Accepted 6 April 2016

Edited by R. A. Pauptit, Macclesfield, England

Keywords: bile salt hydrolase; *Lactobacillus*; lipid metabolism; gut microbiome; crystal structure.

PDB reference: bile salt hydrolase, 5hke

Supporting information: this article has supporting information at journals.iucr.org/f

Bile salt hydrolase (BSH) is a gut-bacterial enzyme that negatively influences host fat digestion and energy harvesting. The BSH enzyme activity functions as a gateway reaction in the small intestine by the deconjugation of glycine-conjugated or taurine-conjugated bile acids. Extensive gut-microbiota studies have suggested that BSH is a key mechanistic microbiome target for the development of novel non-antibiotic food additives to improve animal feed production and for the design of new measures to control obesity in humans. However, research on BSH is still in its infancy, particularly in terms of the structural basis of BSH function, which has hampered the development of BSH-based strategies for improving human and animal health. As an initial step towards the structure–function analysis of BSH, C-terminally His-tagged BSH from *Lactobacillus salivarius* NRRL B-30514 was crystallized in this study. The 1.90 Å resolution crystal structure of *L. salivarius* BSH was determined by molecular replacement using the structure of *Clostridium perfringens* BSH as a starting model. It revealed this BSH to be a member of the N-terminal nucleophile hydrolase superfamily. Crystals of apo BSH belonged to space group $P2_12_12$, with unit-cell parameters a = 90.79, b = 87.35, c = 86.76 Å (PDB entry 5hke). Two BSH molecules packed perfectly as a dimer in one asymmetric unit. Comparative structural analysis of *L. salivarius* BSH also identified potential residues that contribute to catalysis and substrate specificity.

1. Introduction

Microbiota residing in the intestine affect host physiology and growth performance *via* food digestion, nutrient utilization and host immunity modulation. Recent studies have indicated that gut microbiota are implicated in host energy regulation and the development of obesity in humans; thus, manipulating specific gut microbial functions may be one means to control obesity and its associated chronic diseases (DiBaise *et al.*, 2008; Tilg *et al.*, 2009). The intestinal bile salt hydrolase (BSH), an enzyme produced by diverse gut microflora, catalyzes the essential gateway reaction in the metabolism of bile acids in the small intestine and plays an important role in host metabolism and energy harvesting (Begley *et al.*, 2006; Jones *et al.*, 2008; Joyce, Shanahan *et al.*, 2014; Martoni *et al.*, 2015). Using a controlled system, Joyce, MacSharry *et al.* (2014) recently obtained direct evidence demonstrating that BSH activity alone can significantly influence host lipid metabolism and weight gain. Consistent with the findings from this research in humans and mice, extensive research using food animals has shown that the growth-promoting effect of antibiotic growth

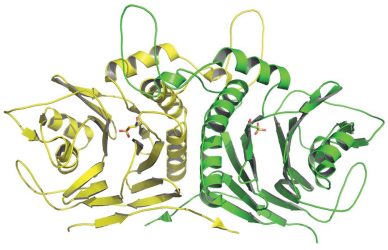

Table 1
Macromolecule-production information for *ls*BSH.

Source organism	*L. salivarius* NRRL B-30514
DNA source	Genomic DNA
Forward primer†	5′-CGCGGATCCATGTGTACAGCAATTACTTT-3′
Reverse primer‡	5′-CCGCTCGAGATTCAACTTATTTATTATTTGT-3′
Cloning vector	pET-21b
Expression vector	pET-21b
Expression host	*E. coli* BL21 (DE3)
Complete amino-acid sequence of the construct produced§	MCTAITLNGNSNYFGRNLDLDFSYGEEVIITPAEY-EFKFRKEKAIKNHKSLIGVGIVANDYPLYFDAI-NEDGLGMAGLNFPGNAYYSDALENDKDNITPFE-FIPWILGQCSDVNEARNLVEKINLINLSFSEQL-PLAGLHWLIADREKSIVVEVTKSGVHIYDNPIG-ILTNNPEFNYQMYNLNKYRNLSISTPQNTFSDS-VDLKVDGTGFGGIGLPGDVSPESRFVRATFSKL-NSSKGMTVEEDITQFFHILGTVEQIKGVNKTES-GKEEYTVYSNCYDLDNKTLYYTTYENRQIVAVT-LNKDKDGNRLVTYPFERKQIINKLNLERHHHHHH

† The BamHI site is underlined. ‡ The XhoI site is underlined. § The His tag is underlined.

promoters (AGPs) is highly correlated with decreased BSH activity as well as a significantly reduced population of *Lactobacillus* species, which are the major BSH producers in the intestine (Lin, 2014). Thus, BSH inhibitors have been proposed as promising feed additives to replace AGPs in order to enhance food safety and the productivity of food animals (Lin, 2014; Wang *et al.*, 2012). Together, these recent findings have strongly suggested that BSH is a key mechanistic microbiome target for the development of novel alternatives to AGPs to enhance animal production and of new measures to control obesity in humans.

The BSH enzyme catalyzes the deconjugation of glycine-conjugated or taurine-conjugated bile acids, which is an essential gateway reaction in the metabolism of bile acids in the small intestine (Begley *et al.*, 2006). The bile acids have dual digestive and signalling roles in the host; therefore, it has increasingly been recognized that intestinal BSH activity has a significant impact on host physiology by disturbing conjugated bile acid-mediated fat metabolism and endocrine functions (Begley *et al.*, 2006; Jones *et al.*, 2008; Joyce, Shanahan *et al.*, 2014; Martoni *et al.*, 2015). A number of BSH enzymes have been identified from different commensal bacteria, and *Lactobacillus* populations are the major BSH producers in the intestine. Despite recent significant progress in the characterization of diverse BSH enzymes, research on BSH is still in its infancy, particularly in terms of the structural basis of BSH function (Begley *et al.*, 2006; Patel *et al.*, 2010). To date, crystal structures of BSH enzymes from only two specific species, *Bifidobacterium longum* and *Clostridium perfrigens*, have been reported (Kumar *et al.*, 2006; Rossocha *et al.*, 2005). Given the ecological diversity of BSH in the gut microbiome, structural analyses of BSH enzymes from various species are warranted, and would lead to the discovery of the critical residues in catalysis and provide key information on the substrate selectivity of BSH enzymes (Begley *et al.*, 2006). Clearly, structural studies on BSH will also directly facilitate future translational research, such as the use of molecular docking to develop BSH inhibitor-based alternatives to AGPs for growth promotion in food animals (Lin, 2014).

Table 2
Crystallization conditions for *ls*BSH.

Method	Sitting-drop vapour diffusion
Plate type	Swissci SD-3
Temperature (K)	293
Protein concentration (mg ml^{-1})	16.0
Buffer composition of protein solution	10 m*M* sodium acetate pH 5.5, 400 m*M* NaCl, 1 m*M* DTT, 1 m*M* EDTA, 10% glycerol
Composition of reservoir solution	20% polyethylene glycol 3350, 0.2 *M* potassium dihydrogen phosphate pH 4.8
Volume and ratio of drop	200 nl, 1:1
Volume of reservoir (µl)	15

Recently, we have identified and characterized a BSH enzyme from *L. salivarius* NRRL B-30514 (Wang *et al.*, 2012). *L. salivarius* BSH (*ls*BSH) was able to efficiently hydrolyze both glycoconjugated and tauroconjugated bile salts. Thus, unlike many BSH enzymes from other bacteria, which have a narrow substrate spectrum, this BSH displayed potent hydrolytic activity towards a broad range of substrates (Wang *et al.*, 2012). The broad substrate specificity of *ls*BSH makes it an ideal candidate for structure–function analysis and for the identification of desired BSH inhibitors using computational techniques. Here, we report the crystallization, X-ray diffraction analysis and structure of *ls*BSH.

2. Materials and methods

2.1. Macromolecule production

Recombinant *ls*BSH was produced in *Escherichia coli* using the pET-21b vector (Novagen). The cloning and purification were described in a recent publication (Wang *et al.*, 2012). The key information for *ls*BSH production is briefly summarized in Table 1. Recombinant *ls*BSH protein, containing a 6×His tag at the C-terminus, was overproduced in *E. coli* BL21 (DE3) cells and subsequently purified using a modified procedure. Briefly, the *E. coli* cells were grown in LB medium containing 100 µg ml^{-1} ampicillin at 37°C until the OD_{600} reached 0.6–0.8. Expression of *ls*BSH was induced by the addition of isopropyl β-D-1-thiogalactopyranoside (IPTG) to a final concentration of 0.5 m*M*. The growth temperature was decreased to 15°C after induction and the culture was further grown for approximately 16 h. Subsequently, the cells were harvested by centrifugation at 5000*g* at 4°C for 20 min and the pellets were resuspended in lysis buffer consisting of 50 m*M* Tris–HCl pH 7.0, 500 m*M* NaCl, 5%(*v*/*v*) glycerol, 50 m*M* imidazole. The resuspended cells were then lysed using a Microfluidics high-pressure homogenizer and centrifuged at 18 000 rev min^{-1} for 1 h at 277 K. The supernatant was subjected to the following stepwise purification. Firstly, the supernatant was loaded onto an Ni–NTA column and washed with a buffer consisting of 50 m*M* Tris–HCl pH 7.0, 50 m*M* NaCl, 5%(*v*/*v*) glycerol, 50 m*M* imidazole. The His-tagged *ls*BSH was eluted with a buffer consisting of 50 m*M* Tris–HCl pH 7.0, 50 m*M* NaCl, 5%(*v*/*v*) glycerol, 150 m*M* imidazole. The purified *ls*BSH fractions from the Ni–NTA column were then subjected to Mono Q chromatography and eluted with a

Table 3
Data-collection and processing statistics for *ls*BSH.

Values in parentheses are for the outer shell.

Diffraction source	Rigaku F-RE^{++}
Wavelength (Å)	1.5418
Temperature (K)	100
Detector	Saturn 944 CCD
Crystal-to-detector distance (mm)	50
Rotation range per image (°)	0.75
Total rotation range (°)	150
Exposure time per image (s)	30
Space group	$P2_12_12$
a, b, c (Å)	90.79, 87.36, 86.77
α, β, γ (°)	90, 90, 90
Mosaicity (°)	0.695
Resolution range (Å)	50.0–1.90 (1.93–1.90)
Total No. of reflections	312064
No. of unique reflections	54757
Completeness (%)	99.3 (90.0)
Multiplicity	5.7 (3.6)
$\langle I/\sigma(I)\rangle$	28.9 (4.91)
$R_{\rm r.i.m.}$	0.060 (0.278)
Overall B factor from Wilson plot (Å^2)	13.0

Table 4
Structure solution and refinement of *ls*BSH.

Values in parentheses are for the outer shell.

PDB code	5hke
Resolution range (Å)	45.50–1.90 (1.97–1.90)
Completeness (%)	99.20 (91.47)
σ Cutoff	2.0
No. of reflections, working set	52091 (2619)
No. of reflections, test set	2619 (213)
Final $R_{\rm cryst}$	0.152 (0.194)
Final $R_{\rm free}$	0.185 (0.218)
No. of non-H atoms	
Protein	5132
Ligand	20
Water	400
Total	5552
R.m.s. deviations	
Bonds (Å)	0.020
Angles (°)	1.877
Average B factors (Å^2)	
Overall	19.8
Protein	19.7
Water	24.9
Ramachandran plot	
Most favoured (%)	97.6
Allowed (%)	2.2
Disallowed (%)	0.2

gradient of sodium chloride [the buffer consisted of 50 m*M* Tris–HCl pH 7.0, 1 *M* NaCl, 5%(*v*/*v*) glycerol, 2 m*M* DTT with a 1–60% gradient of sodium chloride in 20 column volumes (CV)]. Subsequently, the pooled *ls*BSH fractions were further purified using hydrophobic interaction chromatography on a phenyl column; the column was washed with buffer consisting of 50 m*M* Tris pH 7.0, 0.5 *M* NaCl, 5% glycerol, 2 m*M* DTT, and *ls*BSH was eluted using a 10 CV gradient to a buffer consisting of 50 m*M* Tris–HCl pH 7.0, 5%(*v*/*v*) glycerol. Finally, the *ls*BSH fractions were pooled and concentrated to about 3 mg ml^{-1} for purification by Superdex 200 chromatography. *ls*BSH protein with high purity was eluted with buffer consisting of 10 m*M* sodium acetate pH 5.5, 400 m*M* NaCl, 1 m*M* DTT, 1 m*M* EDTA, 10%(*v*/*v*) glycerol.

After purification, the purity of the *ls*BSH was judged using 12% SDS–PAGE as described previously (Wang *et al.*, 2012). The purified *ls*BSH was extensively dialysed against buffer consisting of 10 m*M* sodium acetate pH 5.5, 400 m*M* NaCl, 1 m*M* DTT, 1 m*M* EDTA, 10%(*v*/*v*) glycerol and was then concentrated to 16.0 mg ml^{-1} for crystallization as described below.

2.2. Crystallization

Crystal screening was performed at 293 K by the sitting-drop vapour-diffusion method. 200 nl purified *ls*BSH at a final concentration of 16.0 mg ml^{-1} in buffer consisting of 10 m*M* sodium acetate pH 5.5, 400 m*M* NaCl, 1 m*M* DTT, 1 m*M* EDTA, 10% glycerol was mixed with 200 nl reservoir solution and equilibrated against 15 µl reservoir solution using a Mosquito LCP (TTP Labtech). Commercial crystallization kits from Hampton Research and Qiagen were used for crystal screening. Initial crystals of *ls*BSH were obtained in a condition consisting of 0.2 *M* KH_2PO_4 pH 4.8, 20%(*w*/*v*) polyethylene glycol 3350 and further optimization was carried out by micro-seeding under the same condition. Crystallization information is summarized in Table 2.

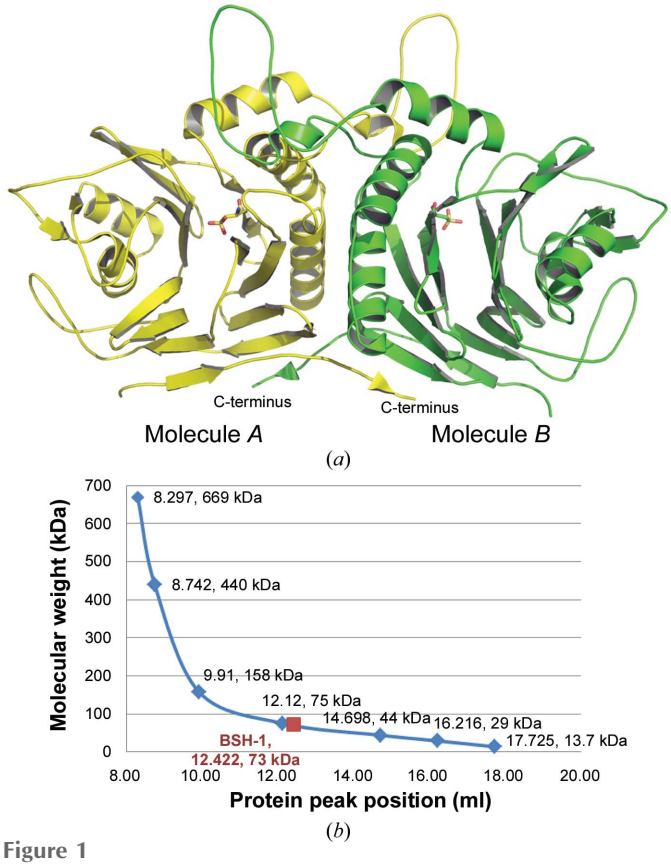

Figure 1
(*a*) Two *ls*BSH molecules packed in one asymmetric unit. The N-terminal Cys2 was oxidized to a cysteinesulfonic acid. (*b*) The dimeric nature of apo *ls*BSH was confirmed by gel filtration on Superdex 200. The solid maroon square shows the position of *ls*BSH (labelled 'BSH-1' in the figure) with an estimated molecular weight of 73 kDa.

Table 5
Major amino-acid residues of *ls*BSH that are potentially involved in catalysis and substrate specificity based on comparative structural analysis.

Residue	Specific location	Speculation
Tyr24	Loop I	Along with Phe65, may force the substrate to sit deeply in the binding pocket
Leu18	Loop I	Given their differences when compared with the structures of *cp*BSH and *bl*BSH, they may contribute to different enzyme–substrate interactions
Phe22	Loop I	
Leu134	Loop II	Both residues contribute to restraint of the spatial configuration by condensing the substrate-binding pocket entrance
Phe130	Loop II	
Ile56	Bottom of the binding pocket	Compared with the structures of *cp*BSH and *bl*BSH, these two residues may determine the differing substrate specificities
Leu63	Bottom of the binding pocket	
Phe65	Bottom of the binding pocker	Along with Tyr24, may force the substrate to sit deeply in the binding pocket

2.3. Data collection and processing

All crystals were flash-cooled with the addition of 25% glycerol as a cryoprotectant and diffraction data were collected at Biortus, Jiangyin, People's Republic of China with a home-source diffraction system consisting of a Rigaku F-RE^{++} generator and a Saturn 944 CCD detector. The data-collection statistics are shown in Table 3.

2.4. Structure solution and refinement

The structure of *ls*BSH was determined by the molecular-replacement method using *Phaser* (McCoy *et al.*, 2007) with the *C. perfringens* BSH (*cp*BSH) structure as a search model (Rossocha *et al.*, 2005; PDB entry 2bjf; 37% sequence identity). Structure refinement was performed with *Coot* (Emsley *et al.*, 2010) and *REFMAC*5 (Murshudov *et al.*, 2011) and is summarized in Table 4.

3. Results and discussion

We have determined the 1.90 Å resolution crystal structure of *ls*BSH in space group $P2_12_12$ (PDB entry 5hke). It showed two *ls*BSH molecules packed perfectly as a dimer in the asymmetric unit (Fig. 1*a*). The presence of the dimer in solution was confirmed by gel filtration with Superdex 200 (Fig. 1*b*). Analysis of the protein interfaces with *PISA* showed that *ls*BSH can be stable as a tetramer and as a dimer in solution (Krissinel & Henrick, 2007).

Except for residues 1 and 301–305, which are missing from the structure of *ls*BSH, all amino acids are well defined, including Cys2, which was oxidized to a cysteinesulfonic acid. The overall structure consisted of a four-layered $\alpha\beta\beta\alpha$ core and showed an N-terminal nucleophile (Ntn) hydrolase-like fold, similar to the previously reported structures of *C. perfrigens* BSH (*cp*BSH), *B. longum* BSH (*bl*BSH) and *Lysinibacillus sphaericus* penicillin V acylase (*bs*PVA) (Kumar *et al.*, 2006; Rossocha *et al.*, 2005; Suresh *et al.*, 1999; Fig. 2).

A superimposition of the structure of *ls*BSH with those of *cp*BSH and *bl*BSH shows that they share the conserved catalytic active centre containing the cysteine nucleophile (Cys2) and its coordinated neighbouring amino acids (Kumar *et al.*, 2006; Rossocha *et al.*, 2005). However, the amino acids surrounding the binding pocket are inconsistent (Fig. 3). Differences were mainly observed in the amino acids within two loops: loop I consisting of amino acids 20–27 and loop II consisting of amino acids 125–139 (residue numbers from *ls*BSH; Fig. 3*a*). Loop II of *ls*BSH is closer to the taurodeoxycholate than that in the *cp*BSH complex structure (PDB entry 2bjf). In loop II the hydrophobic residue Leu134 in *ls*BSH intrudes into the pocket and condenses the entrance to the substrate-binding pocket (Fig. 3*b*). Phe130 may also contribute to this restrained spatial configuration (Fig. 3*b*). In loop I, Tyr24 in *ls*BSH (corresponding to Phe26 in *cp*BSH), along with Phe65 (corresponding to Ala68 in *cp*BSH), also intrudes into the binding pocket (Fig. 3*c*). These observations suggest that these amino acids may force the substrate to bind in a different orientation, such as that rotated by 90°, and to sit deeply in the binding pocket, which will lead to different enzyme–substrate interactions and is obviously different from what was observed in *cp*BSH (Rossocha *et al.*, 2005). In *bl*BSH, which exhibits a preference for glycoconjugated bile salts over tauroconjugated bile salts (Kumar *et al.*, 2006), Tyr24 is present in loop I as observed in *ls*BSH; however, the large hydrophobic amino acid Trp21 (corresponding to Leu20 in *ls*BSH and Ile22 in *cp*BSH) seems to make this tyrosine point outwards from the binding pocket (Fig. 3*c*). In addition to the differences observed in these two loops as described above, comparison of *ls*BSH with *cp*BSH and *bl*BSH also identified differences in other surrounding amino acids in *ls*BSH, including Leu63 (corresponding to Thr66 in *cp*BSH and Met65

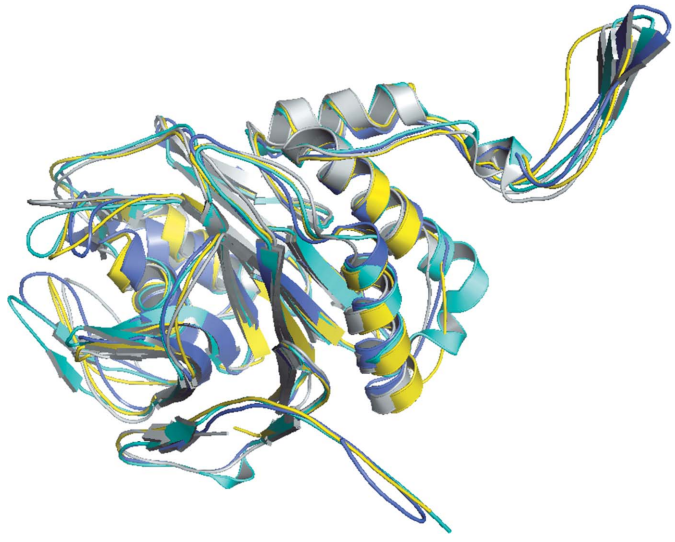

Figure 2
Structural superimposition of *ls*BSH (yellow; PDB entry 5hke) with *cp*BSH (cyan; PDB entry 2bjf), *bl*BSH (grey; PDB entry 2hf0) and *L. sphaericus* penicillin V acylase (slate; PDB entry 3pva).

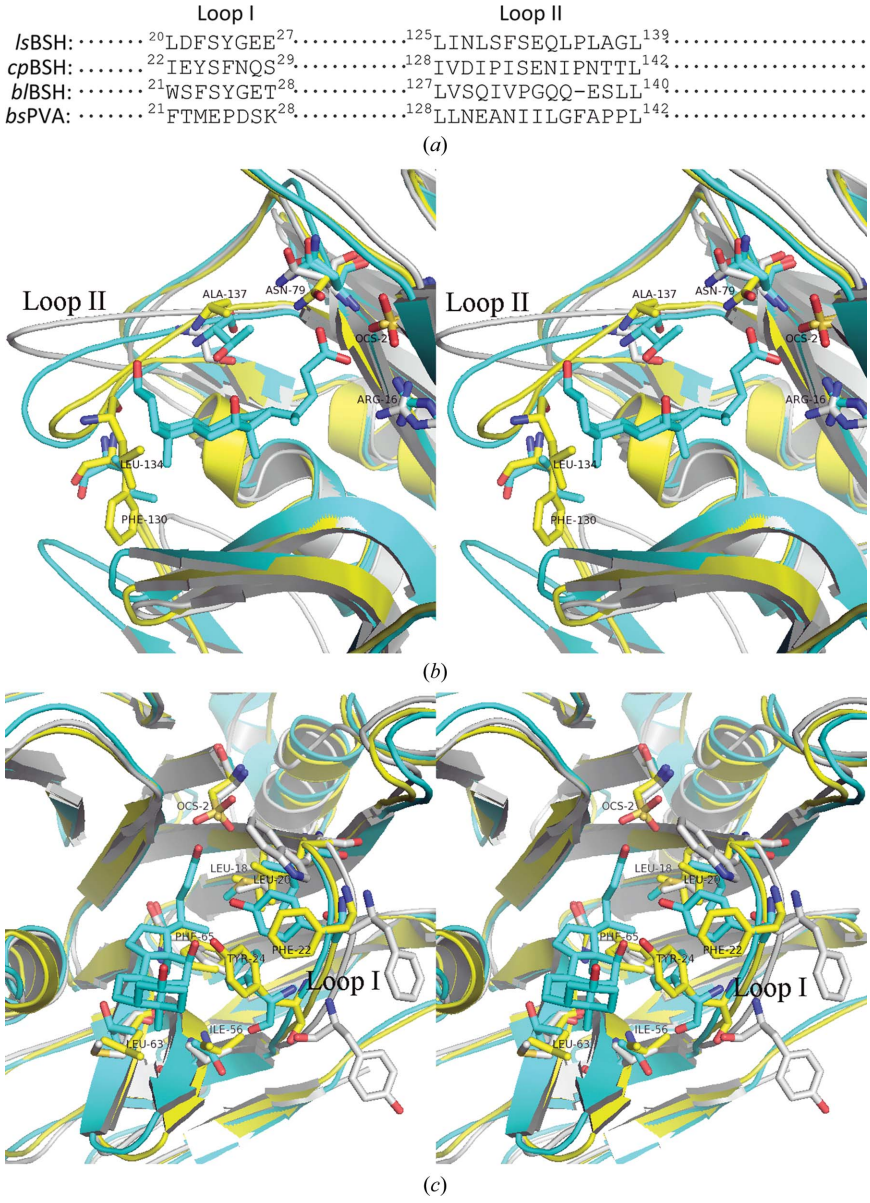

Figure 3
Comparison of the substrate-binding pocket of *ls*BSH (yellow) with those of *cp*BSH (cyan) and *bl*BSH (grey). A reference taurodeoxycholate molecule (cyan) from the *cp*BSH complex structure (PDB entry 2bjf) is shown. (*a*) Sequence alignment of loop I and loop II that surround the binding pocket. (*b*) Cross-eyed stereoview showing the significant difference in loop II. Only the residue numbers for *ls*BSH are shown. (*c*) Cross-eyed stereoview showing the difference in loop I. Only the residue numbers for *ls*BSH are shown.

in *bl*BSH) and Ile56 (corresponding to Thr59 in *cp*BSH and Val58 in *bl*BSH) located at the bottom of the binding pocket, and Phe22 (corresponding to Tyr24 in *cp*BSH and Phe23 in *bl*BSH) and Leu18 (corresponding to Met20 in *cp*BSH and Leu19 in *bl*BSH) located in loop I (Fig. 3*c*). These differences may also contribute to the different enzyme–substrate interactions, consequently determining the different substrate specificities. Together, unlike the binding pocket in *cp*BSH that shows an open entrance with a shallow bottom, a number of unique residues in *ls*BSH make *ls*BSH display a narrow entrance to the binding pocket and an increased inner capacity of the binding pocket, which may enable the substrate to sit deeply in the pocket with a different conformation and lead to the different enzyme–substrate interaction (broad spectrum of specificity); these residues are summarized in Table 5.

Previous comparative genomics and structural studies have identified several conserved, catalytically important residues in the active site of BSH (Cys2, Arg16, Asp19, Asn79, Asn171 and Arg224); however, this conclusion was primarily based on comparison of the structure of BSH with that of penicillin V acylase (Begley *et al.*, 2006; Kumar *et al.*, 2006; Wang *et al.*, 2012). To date, Cys2 is the only residue that has been subjected to site-directed mutagenesis and validated for its essential role in the activity of BSH (Kumar *et al.*, 2006). Therefore, future in-depth structural analysis of *ls*BSH (*e.g.* in complex with a specific substrate) in conjunction with comprehensive amino-

acid substitution mutagenesis would help us to discover the critical residues in catalysis and to understand why *ls*BSH displays a potent catalytic activity towards a broad spectrum of substrates including both glycoconjugated and tauro-conjugated bile salts.

Acknowledgements

This work was supported by the National Natural Science Foundation of China (31172344), the Special Program on Science and Technology Innovation Capacity Building of BAAFS (KJCX20150703) and AgResearch at The University of Tennessee. We also thank the staff of Biortus, Jiangyin, People's Republic of China for assisting us with the crystallization and the collection of high-resolution X-ray data.

References

Begley, M., Hill, C. & Gahan, C. G. M. (2006). *Appl. Environ. Microbiol.* **72**, 1729–1738.

DiBaise, J. K., Zhang, H., Crowell, M. D., Krajmalnik-Brown, R., Decker, G. A. & Rittmann, B. E. (2008). *Mayo Clin. Proc.* **83**, 460–469.

Emsley, P., Lohkamp, B., Scott, W. G. & Cowtan, K. (2010). *Acta Cryst.* D**66**, 486–501.

Jones, B. V., Begley, M., Hill, C., Gahan, C. G. M. & Marchesi, J. R. (2008). *Proc. Natl Acad. Sci. USA*, **105**, 13580–13585.

Joyce, S. A., MacSharry, J., Casey, P. G., Kinsella, M., Murphy, E. F., Shanahan, F., Hill, C. & Gahan, C. G. M. (2014). *Proc. Natl Acad. Sci. USA*, **111**, 7421–7426.

Joyce, S. A., Shanahan, F., Hill, C. & Gahan, C. G. M. (2014). *Gut Microbes*, **5**, 669–674.

Krissinel, E. & Henrick, K. (2007). *J. Mol. Biol.* **372**, 774–797.

Kumar, R. S., Brannigan, J. A., Prabhune, A. A., Pundle, A. V., Dodson, G. G., Dodson, E. J. & Suresh, C. G. (2006). *J. Biol. Chem.* **281**, 32516–32525.

Lin, J. (2014). *Front. Microbiol.* **5**, 33.

Martoni, C. J., Labbé, A., Ganopolsky, J. G., Prakash, S. & Jones, M. L. (2015). *Gut Microbes*, **6**, 57–65.

McCoy, A. J., Grosse-Kunstleve, R. W., Adams, P. D., Winn, M. D., Storoni, L. C. & Read, R. J. (2007). *J. Appl. Cryst.* **40**, 658–674.

Murshudov, G. N., Skubák, P., Lebedev, A. A., Pannu, N. S., Steiner, R. A., Nicholls, R. A., Winn, M. D., Long, F. & Vagin, A. A. (2011). *Acta Cryst.* D**67**, 355–367.

Patel, A. K., Singhania, R. R., Pandey, A. & Chincholkar, S. B. (2010). *Appl. Biochem. Biotechnol.* **162**, 166–180.

Rossocha, M., Schultz-Heienbrok, R., von Moeller, H., Coleman, J. P. & Saenger, W. (2005). *Biochemistry*, **44**, 5739–5748.

Suresh, C. G., Brannigan, J. A., Pundle, A. V., SivaRaman, H., Rao, K. N., McVey, C. E., Verma, C. S., Dauter, Z., Dodson, E. J. & Dodson, G. G. (1999). *Nature Struct. Biol.* **6**, 414–416.

Tilg, H., Moschen, A. R. & Kaser, A. (2009). *Gastroenterology*, **136**, 1476–1483.

Wang, Z., Zeng, X., Mo, Y., Smith, K., Guo, Y. & Lin, J. (2012). *Appl. Environ. Microbiol.* **78**, 8795–8802.